Nanoscale

Accepted Manuscript

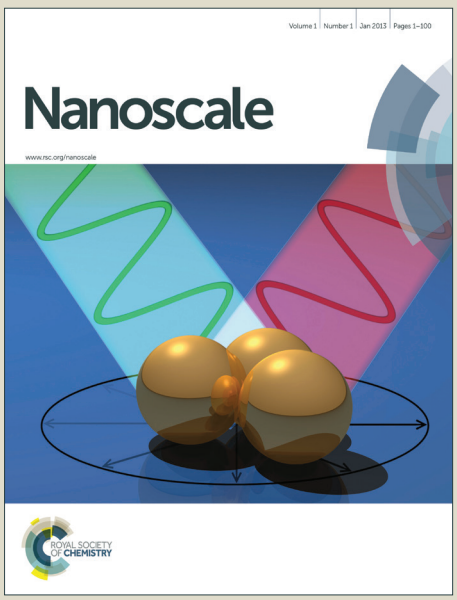

ROYAL SOCIETY OF CHEMISTRY

www.rsc.org/nanoscale

Nanoscale

ARTICLE

Efficient ternary organic photovoltaics incorporating graphene-based porphyrin molecule as a universal electron cascade material†

Received 00th January 20xx,
Accepted 00th January 20xx

DOI: 10.1039/x0xx00000x

www.rsc.org/nanoscale

M. M. Stylianakis,[a,b*] D. Konios,[a,b] G. Kakavelakis,[a,c] G. Charalambidis,[d] E. Stratakis,[c,e] A. G. Coutsolelos,[d*] E. Kymakis[a*] and S. H. Anastasiadis[b, e]

A graphene-based porphyrin molecule (GO-TPP) was synthesized by covalent linkage of graphene oxide (GO) with 5-(4-aminophenyl)-10,15,20-triphenyl) porphyrin (TPP-NH_2). The yielded graphene-based material is a donor-acceptor (D-A) molecule, exhibiting strong intermolecular interaction between the GO core (A) and the covalently anchored porphyrin molecule (D). To demonstrate the universal role of GO-TPP as electron cascade material, ternary blend organic photovoltaics based on [6,6]-phenyl-C_{71}-butyric-acid-methyl-ester ($PC_{71}BM$) as electron acceptor material and two different polymer donor materials, the poly [N-9'-hepta-decanyl-2,7-carbazole-alt-5,5-(40,70-di-2-thienyl-20,10,30-benzothiadiazole)] (PCDTBT) and the high efficient poly ({4,8-bis[(2-ethylhexyl)oxy]benzo[1,2-b:4,5-b']dithiophene-2,6-diyl}{3-fluoro-2-[(2-ethylhexyl) carbonyl]thieno [3,4-b]thiophenediyl} (PTB7), were fabricated. The addition of GO-TPP into the active layer implies continuous percolation paths between the D-A interfaces, enhancing charge transport, reducing exciton recombination and thus improving the photovoltaic performance of the device. A simultaneous increase of short circuit current density (J_{sc}), open-circuit voltage (V_{oc}) and fill factor (FF), compared to PTB7:$PC_{71}BM$ reference cell, led to an improved power conversion efficiency (PCE) of 8.81% for the PTB7: GO-TPP:$PC_{71}BM$-based device, owing mainly to the more efficient energy level offset between the active layer components.

Introduction

Organic photovoltaics (OPVs) are of tremendous interest as a lightweight and flexible power source, which can be easily integrated in wearable electronics and smart textiles.[1] Bulk heterojunction (BHJ)[2] OPVs based on blends consisting of conjugated polymers as the electron donor (D) and soluble fullerenes as the electron acceptor (A) have dominated the last decades research efforts, achieving ~9% and ~10% power conversion efficiency (PCE) using a single[3-5] and a tandem[6] junction OPVs respectively.

This success was mainly due to the utilization of low band gap polymers with deep highest occupied molecular orbital (HOMO) levels,[7] aiming to higher light harvesting as well as the optimization of the two buffer layers for effective charge collection.[8] Nevertheless, the combination of the polymer short exciton diffusion length (~10 nm) with the low charge carrier mobility between the fullerene and the polymer phase separated layers within the photoactive layer, enhances recombination and trapping of the separated electron and holes.[9,10] A straightforward approach to reduce the recombination is the decrease of the charge transfer energy offsets between the D lowest unoccupied molecular orbital (LUMO) level and the A LUMO level. This can be accomplished by the addition of a third component in the binary blend, which can act as a bridge between the D and A materials, structuring a ternary cascade OPV.[9,11] The cascade material energy levels should first of all exhibit a proper offset with respect to the polymer and the fullerene. At the same time, it should effectively act as an electron acceptor and transporter, when a heterojunction is formed with the D and as an electron donor and hole transporter, when it forms a junction with the fullerene.[12-15]

[a] Center of Materials Technology and Photonics & Electrical Engineering Department, School of Applied Technology, Technological Educational Institute (TEI) of Crete, Heraklion, 71004, Crete, Greece; kymakis@staff.teicrete.gr; stylianakis@staff.teicrete.gr
[b] Dept. of Chemistry, Univ. of Crete, Heraklion, 71003 Crete, Greece
[c] Dept. of Materials Science and Technology, Univ. of Crete, Heraklion, 71003 Crete, Greece
[d] Laboratory of Bioinorganic Chemistry, Chemistry Department, University of Crete, Voutes Campus, 71003 Heraklion, Greece
[e] Institute of Electronic Structure and Laser (IESL), Foundation for Research and Technology-Hellas (FORTH).

† Electronic Supplementary Information (ESI) available: [Cyclic voltammographs of GO-TPP, TGA Thermograms of GO and GO-TPP, AFM micrographs and rms values of PCDTBT:$PC_{71}BM$, Photoluminescence (PL) spectra of PCDTBT:GO-TPP:$PC_{71}BM$ and PTB7:GO-TPP:$PC_{71}BM$] See DOI: 10.1039/b000000x/

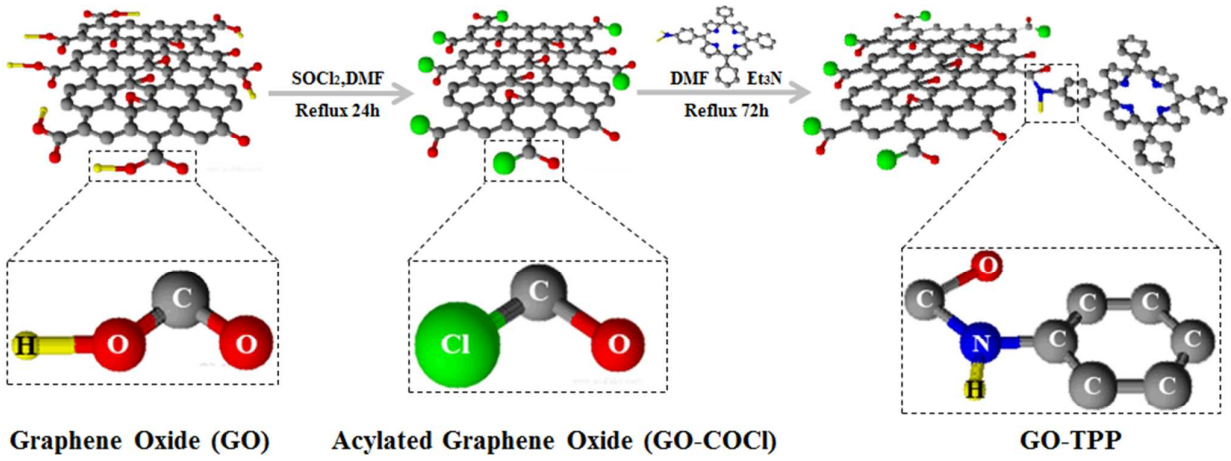

Fig. 1 Schematic representation of the chemical synthesis

Ever since its 2004 isolation,[16] graphene has attracted great interest in the scientific community, promoting its utilization in the various components of novel optoelectronic device.[17-25] In particular, graphene flakes were recently identified as a promising additive for assisting the charge transport in the OPVs photoactive layer[26-29] owing to their excellent charge carrier mobility, thermal and chemical stability, low cost and facile processing.[30] The production of solution processable graphene by exfoliation of graphite into graphene oxide (GO), has allowed the large-scale production of graphene-based devices.[31,32] The presence of oxygen functional groups within the graphene structure, such as hydroxyl (-OH), aldehyde (-CHO), carboxyl (-COOH) or epoxyl ones, reduces the interplane forces and imparts hydrophilic character. Thus, GO is highly soluble in polar organic solvents, forming stable dispersions.[33,34] Moreover, the functional groups can act as promoters for further chemical functionalization of GO based on well-studied carbon surface chemistry.[35,36]

On the other hand, porphyrins exhibit a planar and π-aromatic framework, displaying high photostability, large extinction coefficients, as well as high susceptibility in electron transfer reactions.[37] Similarly, porphyrins have been utilized as the ternary component of D-A active layer, leading to enhancement of the longer wavelengths light-harvesting, extending to the NIR region.[38,39] Therefore, the fine control of the GO functionalization with porphyrin molecules can be advantageous in providing composite materials with LUMO levels between the respective polymer and fullerene ones.

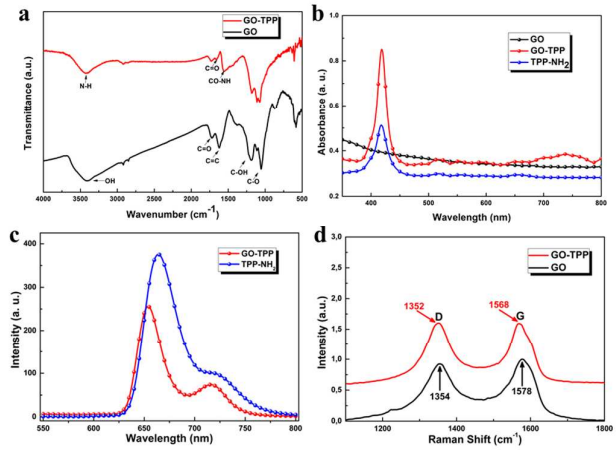

Fig. 2 Characterization of GO (black line) and GO-TPP (red line). a) FT-IR spectra. b) UV-vis spectra including the UV-vis spectrum of TPP-NH_2. c) Room-temperature fluorescence spectra of isoabsorbing (A = 0.24) DMF solutions of TPP-NH_2 (blue line) and GO-TPP (red line) after excitation at 419 nm and d) Raman spectra.

In the present study, GO flakes covalently functionalized with a TPP-NH_2 porphyrin, forming GO-TPP[40-42] composites were incorporated in BHJ polymer:fullerene based OPVs as the electron cascade material. The fine tuning of its energy levels was achieved by adjusting the reaction time of the GO-TPP synthesis, which affected the functionalization degree of the precursor GO-COCl.[29] The universal use of GO-TPP as electron cascade material is demonstrated by using two different polymer donor materials, the poly [N-9'-hepta-decanyl-2,7-carbazole-alt-5,5-(40,70-di-2-thienyl-20,10,30-benzothiadia-zole)](PCDTBT) and the high efficient poly ({4,8-bis[(2-ethylhexyl)oxy]benzo[1,2-b:4,5-b']dithiophene-2,6-diyl}{3-fluoro-2-[(2-ethylhexyl)carbonyl]thieno[3,4-b] thiophenediyl} (PTB7). Record PCEs of 7.13% (~23% enhancement) and 8.81% (~16% enhancement) compared to the binaries PCDTBT:$PC_{71}BM$ and PTB7:$PC_{71}BM$-based OPVs respectively, were achieved, mainly due to the more efficient energy level offset between the ternary active layer components, resulting

in reduced exciton recombination and improved charge transport and collection.

Results and Discussion

Material synthesis and characterization

The covalent linking of GO and TPP-NH_2 occurs between the carboxyl functional side groups of GO and the porphyrin amino groups, forming amide bonds (CONH) (Fig. 1). The synthesis of GO-TPP was carried out by refluxing TPP-NH_2 and GO-COCl in DMF at 130 °C for 72 h in the presence of triethylamine. It is noted that the acylated GO-COCl is extremely sensitive in ambient conditions and therefore it is immediately used in the next reaction step; the covalent linking with the TPP-NH_2 molecule, which is added in excess. The yielded product is washed thoroughly with THF and $CHCl_3$ to remove the excess of TPP-NH_2 and with deionized water to remove the formed Et_3N•HCl. The functional groups as well as the bonds of GO and GO-TPP were identified by FT-IR spectroscopy (Fig. 2a). Primarily, the spectrum of GO (black) displays the -OH stretching vibration as a broad peak at 3390 cm^{-1}. Moreover, the most characteristic features in the FT-IR spectrum of GO are the absorption bands corresponding to the C=O carbonyl stretching at ~1726 cm^{-1}, to C=C graphitic domains at 1622 cm^{-1}, the C-OH stretching at 1220 cm^{-1} and the C-O stretching at 1053 cm^{-1}.[43,44] The spectrum of GO-TPP (red) exhibits a new peak attributed to the amide bond, appeared at 1653 cm^{-1}, corresponding to the characteristic C=O and C-N stretching bands of the amide group, while the peak at ~1726 cm^{-1} of GO is significantly reduced.[45-47] This decrease demonstrates that an important proportion of the GO carboxyl groups is converted to amide bonds.[48]

Fig. 2b shows UV-vis absorption spectra of GO (black), TPP-NH_2 (blue) and GO-TPP (red) in DMF with the GO exhibiting a characteristic absorption band at λ_{max} (DMF ~0.02 mg mL^{-1})/280 nm. The spectra of TPP-NH_2 and GO-TPP appear both strong Soret absorption band at 418 nm and weak Q-bands between 500 and 700 nm, which are consistent with that of porphyrins reported.[40]

In order to investigate the electronic interactions of the porphyrin units with the GO sheets in the excited state, fluorescence spectroscopy was conducted. Upon excitation of TPP-NH_2 and GO-TPP at the Soret band (419 nm), where the absorbance was adjusted to be identical at the excitation wavelength, the characteristic fluorescence emission of TPP-NH_2 was significantly quenched in GO-TPP hybrid material as displayed in Fig. 2c. Except of the quenching, the emission of TPP-NH_2 at 664 nm was also blue shifted by 10 nm to 654 nm. It is difficult to quantify the quenching since the GO, also absorbs at the excitation wavelength. However, the observed emission quenching of the porphyrin indicates that there is a strong interaction between the singlet excited state of the porphyrin and the GO part in the nano-composite material. This quenching may be attributed to either photoinduced electron transfer or energy transfer processes from the porphyrin chromophore to the GO sheets.

An additional proof of GO functionalization was provided by Raman spectroscopy giving both information on the number and orientation of atomic layers of GO, as well as the presence of doping. Fig. 2d depicts the Raman spectra of GO (black line) and GO-TPP (red line). GO Raman spectrum shows two typical broad peaks at 1354 cm^{-1} and 1578 cm^{-1}, corresponding to the defect-induced D and the in-plane vibration of sp^2 carbon G bands, respectively. The functionalized GO with various porphyrins results in small changes in the D and G peaks. Besides this, the D and G bands are shifted from 1354 to 1352 cm^{-1} and 1578 to 1568 cm^{-1}, respectively, which may be a further indication of covalent bonding.[49-51]

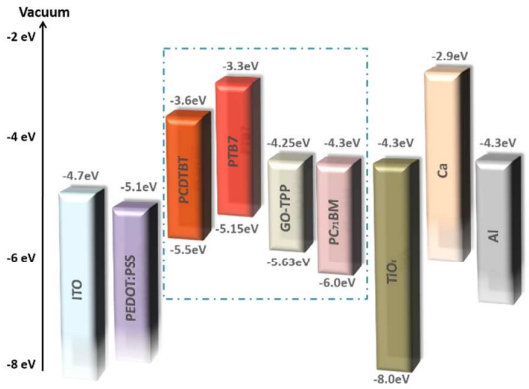

Fig. 3 Energy levels diagram of photovoltaic device components referenced to the vacuum level.

Energy levels of GO-TPP

Cyclic voltammetry (CV) was used to calculate the energy levels of all samples prepared after varying the functionalization degree of GO-COCl, as described in the experimental section. According to the literature, the molecular orbital energy levels can be measured by the voltammographs from the onset potential of the reduction and oxidation process.

The voltammetric behavior of GO-TPP in CH_3CN using 0.1 M ($TBAPF_6$ as the electrolyte, at a scan rate of 10 mV s^{-1}, between the potential sweep window of 1.6 V to -1.6 V is demonstrated in Fig. S1. The energy levels diagram of photovoltaic device components referenced to the vacuum level, are depicted in Fig. 3, where the calculations of HOMO and LUMO levels were based on the following empirical relations from the literature.[52]

$$E_{HOMO} = -(E_{[onset,\ ox\ vs.Fc^+/Fc]} + 5.1)(eV)$$

$$E_{LUMO} = -(E_{[onset,\ red\ vs.Fc^+/Fc]} + 5.1)(eV)$$

Only the electrochemical behavior of GO-TPP composite material synthesized after 72 h is depicted, since the prepared in different reaction times materials did not present any energy levels offset with the D:A pair, as displayed in Table S1. The HOMO level was approximately -5.63 eV calculated by the

oxidation peak onset 0.53 V, while its LUMO level extracted from the onset of the reduction peak (0.85 V) is -4.25 eV. It is clear, that the energy levels of GO-TPP perfectly match the energy levels of polymer donor materials (PCDTBT and PTB7) and $PC_{71}BM$-acceptor, acting as an efficient electron-cascade material.

To evaluate the linked TPP onto the GO backbone sheet, thermogravimetric analysis (TGA) was also used. Fig. S2 displays the TGA curves of GO (black) and GO-TPP (red), respectively. GO begins to lose mass upon heating even below 100 °C, exhibits a rapid mass loss at about 200 °C, probably due to the pyrolysis of labile oxygen-containing functional groups, such as -OH, -CO and -COOH groups, and decomposes above 600 °C, with a total mass loss of ~40% at 800 °C, in agreement with data in the literature.[35] The TGA curve of GO-TPP exhibits approximately a 23% total weight loss, relative to GO. Weight loss between 250 °C and 500 °C is attributed to the loss of TPP molecules covalently attached to GO.[53]

Morphology and charge transport of the composite films

The surface morphologies of the PCDTBT:$PC_{71}BM$ photoactive layer with different weight ratios of GO-TPP (a) 0%; (b) 0.1%; (c)

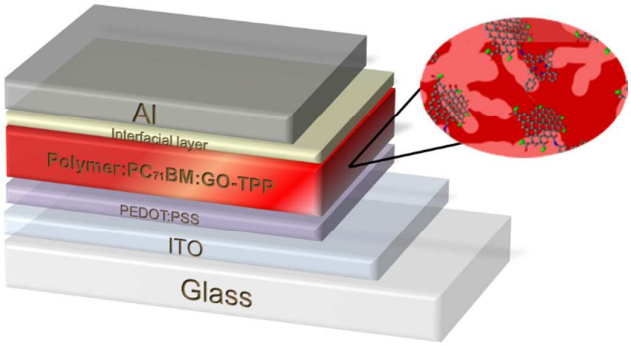

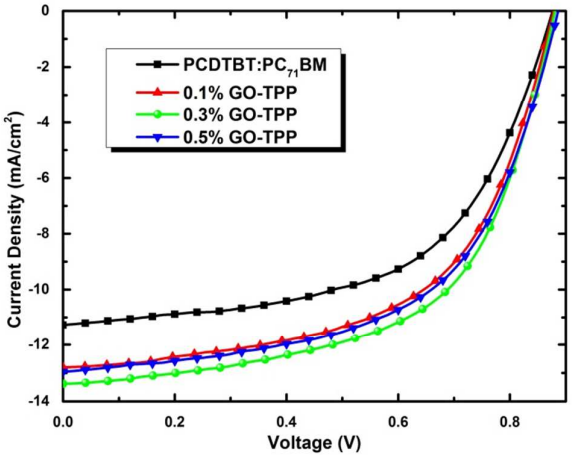

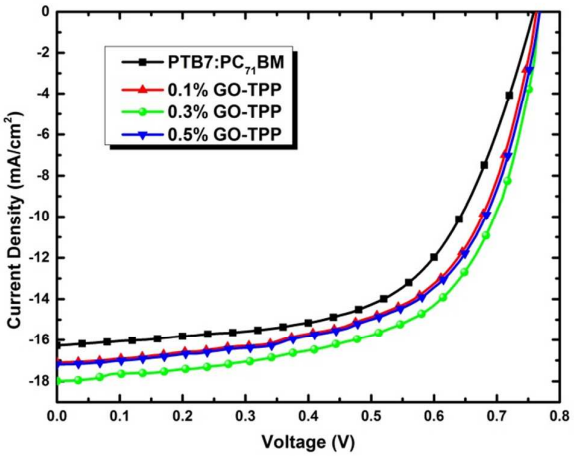

Fig. 4 (Top) Schematic of the photovoltaic device with polymer:$PC_{71}BM$:GO-TPP thin film as the active layer and the structure ITO/PEDOT:PSS/polymer:$PC_{71}BM$:GO-TPP/Interfacial layer/Al. Experimental J–V curves of the photovoltaic devices based on polymer:$PC_{71}BM$ (black curve) and polymer:$PC_{71}BM$:GO-TPP composites (red curve, 0.1%; green curve, 0.3%; blue curve, 0.5%) for PCDTBT (middle) and PTB7 (bottom) polymer donors.

0.3% and (d) 0.5%, respectively, were examined by atomic force microscopy (AFM) with scan size of 5 µm by 5 µm and are displayed as the three-dimensional (3D) AFM images in Fig. S3. It is clear that the side view image of the PCDTBT:$PC_{71}BM$ presents peaks and valleys, giving a root-mean-square (RMS) roughness of 1.13 nm. The incorporation of GO-TPP planarizes the active layer surface roughness, providing smoother surfaces. More specifically, the RMS roughness was consecutively decreased to 0.93 nm and 0.89 nm for PCDTBT:$PC_{71}BM$:GO-TPP composites containing 0.1 and 0.3% GO-TPP, respectively, while was significantly rebounded to 1.37 nm for 0.5% GO-TPP weight ratio.

A series of BHJ photovoltaic devices were fabricated by using GO-TPP as additive material in the photoactive layers. Specifically, different volume ratios of GO-TPP (0.1, 0.3 and 0.5%) were incorporated in the PCDTBT:$PC_{71}BM$ and PTB7:$PC_{71}BM$ blends. The device architecture used ITO/PEDOT:PSS(30 nm)/polymer:GO-TPP:$PC_{71}BM$/Interfacial layer (TiO_x or Ca)/Al (100 nm) is schematically shown in Fig. 4a, while Fig. 4b and 4c display the respective current density-voltage (J-V) curves.

Table 1 displays the photovoltaic characteristics of the fabricated devices, showing that the device containing 0.3% GO-TPP exhibited the best photovoltaic performance both for PCDTBT and PTB7-based devices. In particular, PCDTBT:$PC_{71}BM$:GO-TPP (0.3%)-based device exhibited an open-circuit voltage (V_{oc}) of 0.885 V, J_{sc} of 13.38 mA cm^{-2}, fill factor (FF) of 58.4% and PCE of 6.92%, increased by ~23% compared to the device without the GO-TPP content. In the case of PTB7-based ternary device, the same trend in photovoltaic characteristics was observed with a record PCE of 8.81%. The increase in V_{oc} can be attributed to the higher LUMO level of GO-TPP relative to $PC_{71}BM$, facilitating charge transfer at the D/A interface due to the bridging effect.[12]

As also shown in Table 1, the PTB7-device with 0.5% GO-TPP showed deteriorated characteristics with J_{sc} of ~17.19 mA cm^{-2}, PCE of 8.08% with a V_{oc} of 0.769 V and a FF of 61.2%. It can be postulated that at higher GO-TPP contents, large aggregates were formed, which hindered exciton generation and charge separation and thus leading to lower efficiencies. In order to give further insight on the mechanism responsible for the enhanced photocurrent and performance of the devices, the charges which is detrimental for the device efficiency and thus it is responsible for the increase in J_{sc} and photovoltaic performance. This balance in charge mobilities indicate optimized carrier transport. The presence of DIO additive optimizes the polymer morphology, directly affecting the PTB7:$PC_{71}BM$ interface and increasing the hole mobility of the device.[54] Therefore, the hole/electron mobilities of PTB7-based devices remained almost unchanged upon the GO-TPP addition.

To further support that the GO-TPP molecule in the photoactive layer acts as electron cascade material, enhancing the charge

Table 1 Device performance of photovoltaic devices based on polymer:$PC_{71}BM$:GO-TPP composites with different GO-TPP content*

Polymer	GO-TPP (%)	J_{sc} (mA cm^{-2})	V_{oc} (V)	FF (%)	PCE (%)
PCDTBT	0	11.28±0.21	0.880±0.04	56.7±0.4	5.62±0.18
	0.1	12.80±0.19	0.882±0.05	57.2±0.3	6.46±0.17
	0.3	13.38±0.23	0.885±0.04	58.4±0.5	6.92±0.21
	0.5	12.96±0.21	0.890±0.02	57.2±0.4	6.59±0.17
PTB7	0	16.27±0.23	0.760±0.03	59.8±0.6	7.39±0.21
	0.1	17.09±0.25	0.764±0.03	61.1±0.5	7.97±0.22
	0.3	17.98±0.29	0.767±0.02	62.1±0.6	8.58±0.23
	0.5	17.19±0.25	0.769±0.01	61.2±0.4	8.08±0.19

*The data was averaged from ten identical devices with 6 photovoltaics cells each

Table 2 Hole and electron mobilities of PCDTBT:$PC_{71}BM$:GO-TPP based devices with different GO-TPP content

GO-TPP (%)	μ_h ($cm^2V^{-1}s^{-1}$)	μ_e ($cm^2V^{-1}s^{-1}$)	μ_e/μ_h
0	$9.64\ 10^{-5}$	$2.28\ 10^{-4}$	2.36
0.1	$9.72\ 10^{-5}$	2.2110^{-4}	2.27
0.3	$9.86\ 10^{-5}$	2.1110^{-4}	2.14
0.5	$9.68\ 10^{-5}$	$2.25\ 10^{-4}$	2.32

hole and electron-only space-charge-limited current density (SCLC) were measured (Fig. 5). Electron-only devices based on ITO/Al/PCDTBT:$PC_{71}BM$:GO-TPP/TiO_x/Al and hole-only devices based on ITO/PEDOT:PSS/PCDTBT:$PC_{71}BM$: GO-TPP/MoO_3/Au were fabricated. The SCLC is modelled using the Mott–Gurney equation:

$$J_{SCLC} = \frac{9}{8}\varepsilon_0\varepsilon_r\mu_e\frac{(V-V_{bi})^2}{d^3}$$

where J_{SCLC} is the current density of SCLC, ε_r is the relative permittivity of the organic active layer, ε_0 is the permittivity of free space, V is the applied voltage, V_{bi} is the built-in voltage, μ is the charge mobility, and d is the thickness of the active layer. Thus, by fitting this equation to the experimental data, the charge mobilities of the devices were calculated (Table 2). The addition of the GO-TPP as additive in the active layer balances the values of electron and hole mobilities (Fig. 5 inset). This mobility balance prevents the building up of space

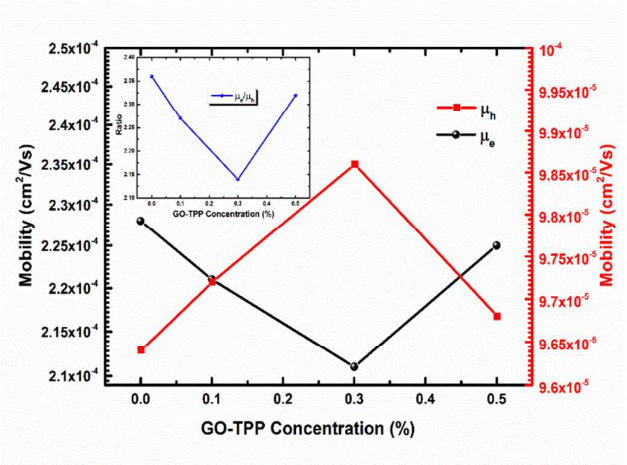

Fig. 5 Electron (black curve) and hole (red curve) mobilities variation upon the addition of GO-TPP. In the inset the electron-to-hole ratio for the different GO-TPP concentration devices is demonstrated.

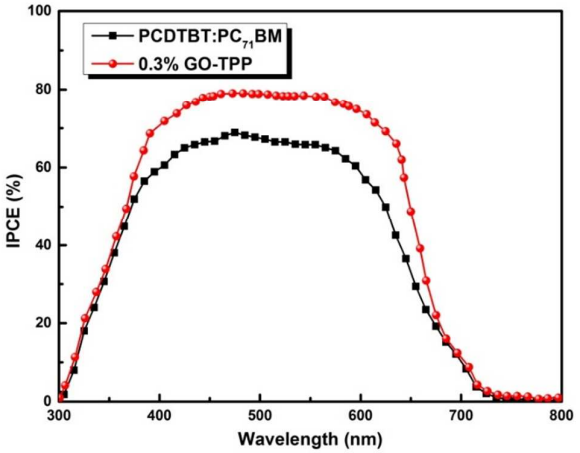

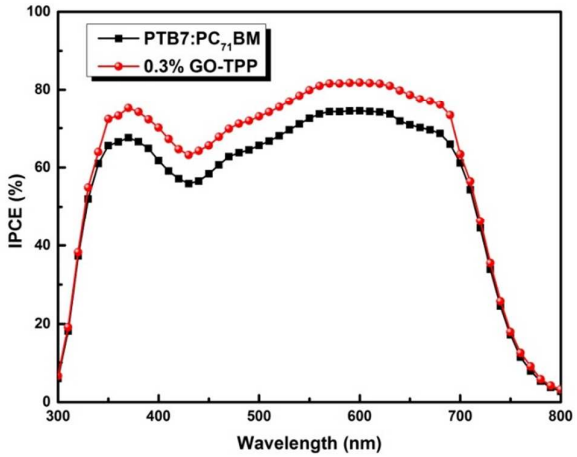

Fig. 6 IPCE curves of the references (black curve) and 0.3% GO-TPP based (red curve) OPV devices. PCDTBT:$PC_{71}BM$ (top) and PTB7$PC_{71}BM$ (bottom).

transport and thus the charge collection, the absorbance and the incident photon-to-electron conversion efficiency (IPCE) curves of the optimum concentration GO-TPP based devices were measured and compared with that of the pristine ones. The addition of GO-TPP in the PCDTBT:$PC_{71}BM$ and PTB7:$PC_{71}BM$ blend solar cells had no significant effect on the light harvesting capability of the devices, owing to the broad absorbance of binary BHJ active layers which screens the absorption contribution of GO-TPP. Furthermore, as shown in Fig. 6, the IPCE enhancement is broad and almost uniform in both ternary BHJ blends, which can be attributed to increased charge transport and collection of the GO-TPP based devices compared to the pristine ones that is due to electron cascade ability of GO-TPP material. It should also be noted that the integrated J_{SC} values from the IPCE spectrum for the PCDTBT:$PC_{71}BM$ and the ternary GO-TPP based devices are 10.95 and 13.44 mA cm^{-2} respectively, while in the PTB7 case are 15.75 and 17.33 mA cm^{-2}. The IPCE calculated values are less than 4% different than the actual measured J_{sc} values, indicating good accuracy of the OPV measurement.

Finally, to evaluate the charge transfer mechanism into the active layers, photoluminescence (PL) measurements were performed at excitation wavelength of 325 nm based on PCDTBT:GO-TPP:$PC_{71}BM$ and PTB7:GO-TPP:$PC_{71}BM$ thin films onto glass/ITO/PEDOT:PSS substrates, respectively (Fig. S4). It is observed that both blends present an emission band around 700 nm corresponding to π–π^* transitions related with the singlet excitons.[55] The photoluminescence quenching is more significant in the PTB7:GO-TPP:$PC_{71}BM$ active layer, owing to the larger energy offset between the LUMO levels of PTB7 and GO-TPP. The PL quenching observed in the ternary device demonstrates that GO-TPP plays a crucial role in the exciton dissociation process.[56] It is clear that the absence of a shift in the PL emission supports the fact that GO-TPP does not contribute to light harvesting but only in charge transfer, in full agreement with absorbance and IPCE measurements.

Experimental Section

Instruments and Measurements

Mid-infrared spectra in the region 500-4000 cm^{-1} were obtained on a Fourier transform infrared (FT-IR) spectrometer (Equinox 55 from Bruker Optics) equipped with a single reflection diamond attenuated-total-reflectance (ATR) accessory (DuraSamp1IR II by Sens IR Technologies). Thermogravimetric analysis (TGA) was performed on 5 mg samples over the temperature range from 40 °C to 800 °C at a heating rate of 10 °C min^{-1} utilizing a Perkin Elmer Diamond Pyris model under nitrogen atmosphere. UV-vis absorption spectra were recorded using a Shimadzu UV-2401 PC spectrophotometer over the wavelength range of 270-800 nm. The emission spectra were measured on a JASCO FP-6500 fluorescence spectrophotometer equipped with a red-sensitive WRE-343 photomultiplier tube (wavelength range 200-850 nm), at room-temperature fluorescence spectra of isoabsorbing (A = 0.24) DMF solutions. The photoluminescence (PL) measurements of ternary active layers were carried out at room temperature and resolved by using a UV grating and a sensitive, calibrated liquid nitrogen cooled CCD camera, in the wavelength range from 600 to 950 nm using a He-Cd CW laser, at 325 nm with a full power of P_0 = 35 mW, as the excitation source. The samples were characterized by Raman spectroscopy at room temperature utilizing a Nicolet Almega XR Raman spectrometer (ThermoScientific) with a 473 nm blue laser as an excitation source. Current-voltage (J-V) measurements were performed at room temperature using an Agilent B1500A Semiconductor Device Analyzer. All electrochemical experiments were carried out by using a model PGSTAT302N (Autolab). The experiments were done with a conventional three electrode electrochemical cell. The three electrode system consisted of Ag/AgCl (SCE) as the reference electrode, Pt-disc as the working electrode and Pt-wire as the counter electrode. Ferrocene (Aldrich, 98%), tetrabutylammonium hexafluorophosphate >99.0% ($TBAPF_6$, Fluka, electrochemical analysis >99%), acetonitrile (Acros Organics, extra dried and distilled >99.9%), were used as received, without further purification. The photovoltaic devices were illuminated with 100 mW cm^{-2} power intensity of white light by an Oriel solar simulator with an A.M. 1.5 G filter. The fabrication of PTB7-based devices was conducted inside a nitrogen filled glove box (MBRAUN) to ensure oxygen (O_2 < 0.1 ppm) and moisture (H_2O < 0.1 ppm) free environment.

Synthesis of Graphene oxide (GO)

GO was prepared from purified natural graphite powder (Alfa Aesar, ~200 mesh) according to a modified Hummers' method.[57] Specifically, graphite powder (0.5 g) was placed into a cold mixture of concentrated H_2SO_4 (40 mL, 98%) and $NaNO_3$ (0.375 g) under vigorous stirring for 1 h, in an ice bath. $KMnO_4$ (3 g) was slowly added into the reaction mixture over 1 h. The mixture was then stirred at room temperature for 4 h. Thereafter, the reaction mixture was allowed to reach room temperature before being heated to 35 °C for 30 min, forming a thick paste. It was then poured into a beaker containing 50

mL of deionized water and further heated to 90 °C for 30 min. 200 mL of distilled water was added, followed by a slow addition of H_2O_2 (3 mL, 30%), turning the color of the solution from dark brown to yellow.

The reaction mixture was then allowed to settle down and decanted. The graphite oxide obtained was then purified by repeated high-speed centrifugation (4200 rpm, 3 min) and redispersing in deionized water to neutralize the pH (~10 times needed). Finally, the resulting GO was dried at 60 °C in a vacuum oven for 48 h.

Synthesis of TPP-NH_2, (5-(4-aminophenyl)-10,15,20-triphenyl) porphyrin

TPP-NH_2 was prepared according to the literature.[58]

Acylation of GO (GO-COCl)

GO (60 mg) was dispersed in $SOCl_2$ (40 mL) and a catalytic amount of DMF (1 mL) was added. The mixture was sonicated, stirred and refluxed for 24 h at 75 °C, under N_2. The excess of thionyl chloride and solvent was removed by distillation under reduced pressure.[59] The obtained solid (GO-COCl) was washed with ultra-dried tetrahydrofuran (THF) three times and dried at 40 °C in a vacuum oven for 30 min.

Synthesis of GO-TPP

An amount of the acylated GO-COCl (40 mg) was dispersed in DMF (20 mL) via ultrasonication treatment for 30 min. Then, TPP-NH_2 (60 mg) in excess was added, in the presence of triethylamine (1 mL) as catalyst. By controlling the reaction time, different functionalization degrees were achieved. For this purpose, the initial mixture was separated into three parts of the same volume. Each sample was stirred and refluxed at 130 °C for 24, 48, 60, 72 and 96 h respectively, under N_2 atmosphere. After the completion of the respective reaction, the solution was cooled at room temperature and then poured into diethylether (~50 mL) to precipitate the product. The product was isolated from the red-purple supernatant by centrifugation (4200 rpm, 5 min). The slushiness precipitate was dried in a vacuum oven at 50 °C for 10 min. Thereafter, it was redispersed in THF (~5 mL) through ultrasonication (10 min), and was centrifuged (4200 rpm, 3 min). The above procedure was repeated 5 times, for each sample, using THF and 5 more using $CHCl_3$, as washing solvents, in order to remove the excess of the unreacted TPP-NH_2. The final product was washed with distilled water (5 times) to remove $Et_3N{\bullet}HCl$ and was left in a vacuum oven for drying (65 °C, 48 h), yielded ~ 50%.

TiO_x solution preparation

Titanium (IV) isopropoxide ($Ti[OCH(CH_3)_2]_4$, 5 mL), 2-methoxyethanol ($CH_3OCH_2CH_2OH$, 20 mL) and ethanolamine ($H_2NCH_2CH_2OH$, 2 mL) were added to a three-necked flask under nitrogen atmosphere. The solution was then stirred for 1 h at room temperature, followed by heating at 80 °C for 1 h and 120 °C for additional 1 h. The solution was then cooled to room temperature and 10 mL of methanol was added.

Fabrication of polymer:$PC_{71}BM$:GO-TPP nanocomposites and measurements of photovoltaic devices

PCDTBT:$PC_{71}BM$ were dissolved in 1,2-dichlorobenzene:chlorobenzene (3:1) (o-DCB:CB) with a 1:4 (4 mg:16 mg) ratio. A PTB7:$PC_{71}BM$ 1:1.5 (10 mg:15 mg) ratio was dissolved in chlorobenzene, followed by the addition of 1,8-diiodooctane (DIO) to give overall DIO amount of 3%. GO-TPP was dispersed in N-Methyl-2-pyrrolidone (NMP) (1 mg mL^{-1}) by ultrasonication for 1 h, in an ultrasonic bath (Elma S 30 H Elmasonic). After ultrasonication, the dispersion was left to settle for 24 h to allow the heavy GO-TPP sheets (with large diameter) to sediment out. The photovoltaic devices reported were fabricated on 20 mm by 15 mm indium-tin-oxide (ITO) glass substrates with a sheet resistance of ~20 Ω sq^{-1}. The impurities are removed from the ITO glass through a 3-step cleaning process. As a hole transport layer, poly(ethylene-dioxythiophene) doped with poly(4-styrenesulfonate) (PEDOT:PSS), purchased from Heraeus, was spin-cast from an aqueous solution on the ITO substrate at 6000 rpm for 60 s and the average thickness of the layer was 30 nm, followed by baking for 15 min at 120 °C inside a nitrogen-filled glove box. Then, GO-TPP dispersion (supernatant) was blended into the PCDTBT:$PC_{71}BM$ (ambient conditions) and PTB7:$PC_{71}BM$ (inert atmosphere) solution and mixed for 2 h. Composite blends with 0.1, 0.3 and 0.5% GO-TPP, were prepared. All photoactive layers were subsequently deposited by spin-coating the blend solutions at 1000 rpm on top of PEDOT:PSS layer. For PCDTBT-based devices, TiO_x interlayer was dissolved in methanol (1:200) and then spin-coated to a thickness of approximately 10 nm (6000 rpm, 40 s) in air.[60] The devices were then heated at 80 °C for 1 min in air. For PTB7-based devices, calcium interfacial layer (2.5 nm) was thermally evaporated. Lastly, 100 nm of Al was deposited through a shadow mask by thermal evaporation on the devices through a shadow mask to define an active area of 4 mm^2 for each device. The performances of the devices were measured at room temperature with an Air Mass 1.5 Global (A.M. 1.5 G) solar simulator at an intensity of 100 mW cm^{-2}. A reference monocrystalline silicon solar cell from Newport was used to calibrate the light intensity. The external quantum efficiency measurements were conducted immediately after device fabrication using an integrated system (Enlitech, Taiwan) and a lock-in amplifier with a current preamplifier under short-circuit conditions. The light spectrum was calibrated using a monocrystalline photodetector of known spectral response. The OPV devices were measured using a Xe lamp passing through a monochromator and an optical chopper at low frequencies (~200 Hz) in order to maximize the sound/noise (S/N) ratio.

Conclusions

We have synthesized a graphene-based material, consisting of GO covalently linked with porphyrin moieties (GO-TPP) which

was thoroughly characterized and incorporated, in different concentrations (0.1, 0.3 and 0.5%), into the active layer of polymer:$PC_{71}BM$, forming ternary blends. The addition of GO-TPP induces a favourable energy alignment between the energy levels of D-A, facilitating the electron-cascade effect. The ideal ternary blend devices based on ITO/PEDOT:PSS/polymer: $PC_{71}BM$:GO-TPP/Interfacial layer/Al structure incorporating two different polymers (PCDTBT and PTB7) and containing 0.3% GO-TPP, resulted to an significant increase of J_{sc}. A PCE of 8.81% in the case of the PTB7-based devices with an enhancement of ~16% was achieved compared to the reference device. The universally applicable role of GO-TPP as an electron cascade material could be demonstrated with the state-of-the-art polymer donor material poly[4,8-bis(5-(2-ethylhexyl)thiophen-2-yl)benzo[1,2-b;4,5-b']dithiophene-2,6-diyl-alt-(4-(2-ethylhexyl)-3- fluorothieno [3,4-b] thiophene-)-2- carboxylate-2-6-diyl)] (PBDTTT-EFT) establishing PCEs over 10% and making an important step to tackle the gap between OPVs and silicon-based counterparts.

Acknowledgements

This research has been cofinanced by the European Union (European Social Fund, ESF) and Greek national funds through the Operational Program "Education and Lifelong Learning" of the National Strategic Reference Framework (NSRF) Research Funding Program: Heracleitus II. Investing in knowledge society through the European Social Fund.

Notes and references

1 M. Kaltenbrunner, M. S. White, E. D. Głowacki, T. Sekitani, T. Someya, N. S. Sariciftci, S. Bauer, *Nat. Commun.* **2012***, 3,* 770.
2 C. J. Brabec, N. S. Sariciftci, J. C. Hummelen, *Adv. Funct. Mater*., 2001, **11**, 15.
3 S. Liu, K. Zhang, J. Lu, J. Zhang, H.-L. Yip, F. Huang, Y. Cao, *J. Am. Chem. Soc.*, 2013, **135**, 15326.
4 S.-H. Liao, H.-J. Jhuo, P.-N. Yeh, Y.-S. Cheng, Y.-L. Li, Y.-H. Lee, S. Sharma, S.-A. Chen, *Sci. Rep.*, 2014, **4**, 6813.
5 S.-H. Liao, H.-J. Jhuo, Y.-S. Cheng, S.-A. Chen, *Adv. Mater.*, 2013, **25**, 4766.
6 J. You, L. Dou, K. Yoshimura, T. Kato, K. Ohya, T. Moriarty, K. Emery, C.-C. Chen, J. Gao, G. Li, Y. Yang, *Nat. Commun.*, 2013, **4**, 1446.
7 Z. He, C. Zhong, X. Huang, W.-Y. Wong, H. Wu, L. Chen, S. Su, Y. Cao, *Adv. Mater.*, 2011, **23**, 4636.
8 Z. He, C. Zhong, S. Su, M. Xu, H. Wu, Y. Cao, *Nat. Photon.*, 2012, **6**, 591.
9 T. Ameri, P. Khoram, J. Min, C. J. Brabec, *Adv. Mater.*, 2013, **25**, 4245.
10 G. Dennler, M. C. Scharber, C. J. Brabec, *Adv. Mater.*, 2009, **21**, 1323.
11 C. Li, Y. Chen, S. A. Ntim, S. Mitra, *Appl. Phys. Lett.*, 2010, **96**, 143303.
12 P. Cheng, Y. Li, X. Zhan, *Energy & Environ. Sci.*, 2014, **7**, 2005.
13 N. A. Cooling, X. Zhou, T. A. Sales, S. E. Sauer, S. J. Lind, K. C. Gordon, T. W. Jones, K. B. Burke, P. C. Dastoor, W. J. Belcher, *Sol. Energy Mater. Sol. Cells*, 2012, **98**, 308.
14 L. Lu, T. Xu, W. Chen, E. S. Landry, L. Yu, *Nat. Photon*., 2014, **8**, 716.
15 L. Yang, L. Yan and W. You, *J. Phys. Chem. Lett.*, 2013, **4**, 1802.
16 K. S. Novoselov, A. K. Geim, S. V. Morozov, D. Jiang, Y. Zhang, S. V. Dubonos, I. V. Grigorieva, A. A. Firsov, *Science*, 2004, **306**, 666.
17 E. Kymakis, K. Savva, M. M. Stylianakis, C. Fotakis, E. Stratakis, *Adv. Funct. Mater.*, 2013, **23**, 2742.
18 G. Kakavelakis, D. Konios, E. Stratakis, E. Kymakis, *Chem. Mater*., 2014, **26**, 5988.
19 M. M. Stylianakis, M. Sygletou, K. Savva, G. Kakavelakis, E. Kymakis, E. Stratakis, *Adv. Opt. Mater.*, 2015, **3**, 658.
20 D. Konios, C. Petridis, G. Kakavelakis, M. Sygletou, K. Savva, E. Stratakis, E. Kymakis, *Adv. Funct. Mater.*, 2015, **25**, 2213.
21 Z. Yin, J. Zhu, Q. He, X. Cao, C. Tan, H. Chen, Q. Yan, H. Zhang, *Adv. Energy Mater.*, 2014, **4**, 1300574.
22 Z. Yin, S. Sun, T. Salim, S. Wu, X. Huang, Q. He, Y. M. Lam, H. Zhang, *ACS Nano*, 2010, **4**, 5263.
23 S.-S. Li, K.-H. Tu, C.-C. Lin, C.-W. Chen, M. Chhowalla, *ACS Nano*, 2010, **4**, 3169.
24 C. T. G. Smith, R. W. Rhodes, M. J. Beliatis, K. D. G. I. Jayawardena, L. J. Rozanski, C. A. Mills, S. R. P. Silva, *Appl. Phys. Lett.*, 2014, **105**, 073304.
25 M. J. Beliatis, K. K. Gandhi, L. J. Rozanski, R. Rhodes, L. McCafferty, M. R. Alenezi, A. S. Alshammari, C. A. Mills, K. D. G. I. Jayawardena, S. J. Henley, S. R. P. Silva, *Adv. Mater.*, 2014, **26**, 2078.
26 G. H. Jun, S. H. Jin, B. Lee, B. H. Kim, W.-S. Chae, S. H. Hong and S. Jeon, *Energy Environ. Sci.*, 2013, **6**, 3000.
27 P. Robaeys, F. Bonaccorso, E. Bourgeois, J. D'Haen, W. Dierckx, W. Dexters, D. Spoltore, J. Drijkoningen, J. Liesenborgs, A. Lombardo, A. C. Ferrari, F. Van Reeth, K. Haenen, J. V. Manca, M. Nesladek, *Appl. Phys. Lett.*, 2014, **105**, 083306.
28 C. X. Guo, G. H. Guai, C. M. Li, *Adv. Energy Mater.*, 2011, **1**, 448.
29 F. Bonaccorso, N. Balis, M. M. Stylianakis, M. Savarese, C. Adamo, M. Gemmi, V. Pellegrini, E. Stratakis, E. Kymakis, *Adv. Funct. Mater.*, 2015, **25**, 3870.
30 M. D. Stoller, S. Park, Y. Zhu, J. An, R. S. Ruoff, *Nano Lett.*, 2008, **8**, 3498.
31 G. Eda, G. Fanchini, M. Chhowalla, *Nat. Nanotech.*, 2008, **3**, 270.
32 G. Eda, M. Chhowalla, *Adv. Mater.*, 2010, **22**, 2392.
33 J. I. Paredes, S. Villar-Rodil, A. Martinez-Alonso, J. M. D. Tascon, *Langmuir*, 2008, **24**, 10560.
34 D. Konios, M. Stylianakis, E. Stratakis, E. Kymakis, *J. Colloid Interface Sci.*, 2014, **430**, 108.
35 M. M. Stylianakis, E. Stratakis, E, Koudoumas, E. Kymakis, S. H. Anastasiadis, *ACS Appl. Mater. & Interfaces*, 2012, **4**, 4864.
36 M. M. Stylianakis, G. D. Spyropoulos, E. Stratakis, E. Kymakis, *Carbon*, 2012, **50**, 5554.
37 D. M. Guldi, M. Prato, *Acc. Chem. Res.*, 2000, **33**, 695.
38 L. Lu, T. Xu, W. Chen, E. S. Landry, L. Yu, *Nat. Photon.*, 2014, **8**, 716.
39 J. Kesters, P. Verstappen, M. Kelchtermans, L. Lutsen, D. Vanderzande, W. Maes, *Adv. Energy Mater.*, 2015, **5**, 1500218.
40 Z.-B. Liu, Y.-F. Xu, X.-Y. Zhang, X.-L. Zhang, Y.-S. Chen, J.-G. Tian, *J. Phys. Chem. B*, 2009, **113**, 9681.
41 R. Yamuna, S. Ramakrishnan, K. Dhara, R. Devi, N. K. Kothurkar, E. Kirubha, P. K. Palanisamy, *J. Nanopart. Res.*, 2013, **15**, 1399.
42 Y. Xu, Z. Liu, X. Zhang, Y. Wang, J. Tian, Y. Huang, Y. Ma, X. Zhang, Y. Chen, *Adv. Mater.*, 2009, **21**, 1275.
43 X. Wang, L. Song, H. Yang, W. Xing, B. Kandola, Y. Hu, *J. Mater. Chem.*, 2012, **22**, 22037.
44 P. V. Kumar, N. M. Bardhan, S. Tongay, J. Wu, A. M. Belcher, J. C. Grossman, *Nat. Chem.*, 2014, **6**, 151.
45 S. Niyogi, E. Bekyarova, M. E. Itkis, J. L. McWilliams, M. A. Hamon, R. C. Haddon, *J. Am. Chem. Soc.*, 2006, **128**, 7720.

46 M. O. Senge, M. Fazekas, E. G. A. Notaras, W. J. Blau, M. Zawadzka, O. B. Locos, E. M. Ni Mhuircheartaigh, *Adv. Mater.*, 2007, **19**, 2737.
47 J. Zhu, J. Yang, B. Deng, *Environ. Chem. Lett.*, 2010, **8**, 277.
48 H. Gunzler and H. U. Gremlich, Winheim: Wiley-VSH, 2002, 223.
49 M. Quintana, K. Spyrou, M. Grzelczak, W. R. Browne, P. Rudolf, M. Prato, *ACS Nano*, 2010, **4**, 3527.
50 K. N. Kudin, B. Ozbas, H. C. Schniepp, R. K. Prud'homme, I. A. Aksay, R. Car, *Nano Lett.*, 2008, **8**, 36.
51 M. Fang, K. Wang, H. Lu, Y. Yanga, S. Nutt, *J. Mater. Chem.*, 2009**, 19**, 7098.
52 C. M. Cardona, W. Li, A. E. Kaifer, D. Stockdale, G. C. Bazan, *Adv. Mater.*, 2011, **23**, 2367.
53 X. Zhang, L. Hou, A. Cnossen, A. C. Coleman, O. Ivashenko, P. Rudolf, B. J. van Wees, W. R. Browne, B. L. Feringa, *Chem. Eur. J.*, 2011, **17**, 8957.
54 S. Foster, F. Deledalle, A. Mitani, T. Kimura, K. B. Kim, T. Okachi, T. Kirchartz, J. Oguma, K. Miyake, J. R. Durrant, S. Doi, J. Nelson, *Adv. Energy Mater.*, 2014, **14**, 1400311.
55 M. Tong, N. E. Coates, D. Moses, A. J. Heeger, S. Beaupré, M. Leclerc, *Physical Review B*, 2010, **81**, 125210.
56 N. A. Nismy, K. D. G. I. Jayawardena, A. A. D. T. Adikaari, S. R. P. Silva, *Adv. Mater.*, 2011, **23**, 3796.
57 Q. Su, S. Pang, V. Alijani, C. Li, X. Feng, K. Mullen, *Adv. Mater.*, 2009, **21**, 3191.
58 K. Ladomenou, T. Lazarides, M. K. Panda, G. Charalambidis, D. Daphnomili, A. G. Coutsolelos, *Inorg. Chem.*, 2012, **51**, 10548.
59 M. M. Stylianakis, J. A. Mikroyannidis, E. Kymakis, *Sol. Energy Mater. Sol. Cells*, 2010, **94**, 267.
60 G. Kakavelakis, E. Stratakis, E. Kymakis, *Chem. Commun.*, 2014, **50**, 5285.